Exciton States in GaAs/AlGaAs Bragg Confining Structures Studied by Resonant Raman Scattering

M. Zahler, E. Cohen, J. Salzman, and E. Linder
Solid State Institute, Technion-Israel Institute of Technology, Haifa 32000, Israel

L. N. Pfeiffer
AT&T Bell Laboratories, Murray Hill, New Jersey 07974
(Received 7 April 1993)

The LO phonon resonant Raman scattering is studied in GaAs/$Al_{0.32}Ga_{0.68}As$ Bragg confining structures and in a similar (reference) superlattice. Strong resonances, with a large outgoing/incoming beam intensity ratio, are observed in the spectral range of the $(e_B{:}hh_B)$ Bragg confined excitons as well as in the $(e_1{:}hh_1)$ exciton band. The resonance profiles are analyzed in terms of a model of exciton scattering by interface and alloy potential fluctuations. The Bragg confined $1S$ excitons are found to be virtually two dimensional, while those of the superlattice are intermediate between two and three dimensions.

PACS numbers: 73.20.Dx, 78.30.Fs, 78.66.Fd

In commonly studied semiconductor quantum wells (QW's) the carriers are confined in the well by their wave function reflection from the barriers. Several recent studies have demonstrated that carriers can be confined in the quantum barrier [1,2], or in the well with an energy higher than that of the barrier [3,4]. The confinement mechanism is then based on two requirements: (a) The carrier wave function must be coherent over a long distance [in the confinement direction, that is, the growth direction (z) of the structures discussed below]. (b) The carrier de Broglie wavelength along the confinement direction must fulfill a certain Bragg reflection condition [5], so that its wave function amplitude outside the barriers is greatly reduced. In such a Bragg confining structure (BCS), properly designed superlattice (SL) sections act as Bragg reflectors [6]. This results in a discrete energy level, corresponding to the barrier-confinement state that falls within the first SL mini stop-band.

In this Letter we present a study of the various exciton states in undoped BCS's by LO phonon resonant Raman scattering (RRS), in which these excitons are the intermediate states. The observed RRS profiles, namely, the scattering intensity dependence on the excitation (laser) energy, are analyzed in terms of anisotropic $1S$ exciton wave functions that are appropriate to the type of confinement. In all these cases the translational motion of the excitons is treated as that of particles that undergo (elastic) scattering by the static potential fluctuations that are due to interface roughness or alloy disorder. By this way we find that Bragg confined excitons can be well described as two-dimensional particles moving solely in the confinement (barrier) layer. We also compare the RRS profile in the spectral range of the $(e_1{:}hh_1)$ exciton in the SL sections (of the BCS) with that of a similar, fully periodic SL. This comparison shows that the excitons are quasi two dimensional in the finite SL sections and closer to three-dimensional particles in the fully periodic SL.

All the structures studied here were grown by molecular beam epitaxy on (001) oriented GaAs substrates. The BCS's consist of SL sections, each one with five periods of eight monolayers (ML) of GaAs wells and 22 ML of $Al_{0.32}Ga_{0.68}As$ barriers. Between these SL sections there are $Al_{0.32}Ga_{0.68}As$ spacers, 66 ML thick. The "unit cell" of this BCS is schematically shown in Fig. 1. It is repeated 60 times. The reference structures is a SL grown within the same parameters as the finite SL sections of the BCS, and its unit cell is repeated 300 times. All samples are undoped. The experimental techniques are detailed in Ref. [1].

The GaAs-like LO phonon RRS profile of the BCS, measured in the spectral range of the $(e_B{:}hh_B)$ exciton is shown in Fig. 2, curve *c*. Also shown are the photoluminescence (PL) spectrum (Fig. 2, curve *a*) and its excitation (PLE) spectrum, monitored in the $(e_1{:}hh_1)$ exciton, at 1.754 eV (Fig. 2, curve *b*). The reference (SL) sample does not show any resonant enhancement in the spectral range of Fig. 2, and the LO phonon Raman

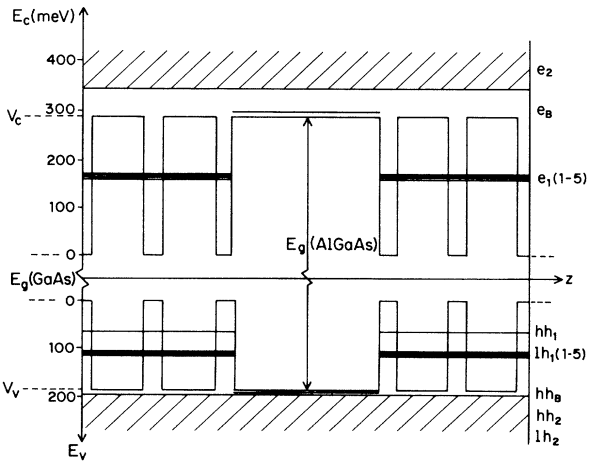

FIG. 1. The one-dimensional "unit cell" of the Bragg confining structure represented by the conduction and valence bands. The band offset ratio is 6:4. Note the Bragg confined states e_B and hh_B in the spacers.

0031-9007/93/71(3)/420(4)$06.00

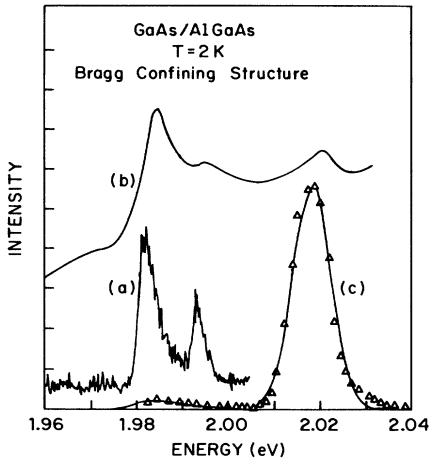

FIG. 2. Curve *a*, the PL spectrum (excited at $E_l = 2.075$ eV) showing the $(e_B{:}hh_B)$ $1S$ band (at 1.98 eV) and the $(e_B{:}lh_B)$ $1S$ band (at 1.991 eV). Curve *b*, the PLE spectrum monitored in the $(e_1{:}hh_1)$ exciton (at 1.754 eV). In addition to the two exciton bands (seen in the PL spectrum) a LO phonon sideband is observed at 2.02 eV. Curve *c*, the GaAs-like LO phonon RRS profile. The triangles are the measured integrated intensities and the solid line is the model calculated with the parameters given in Table I.

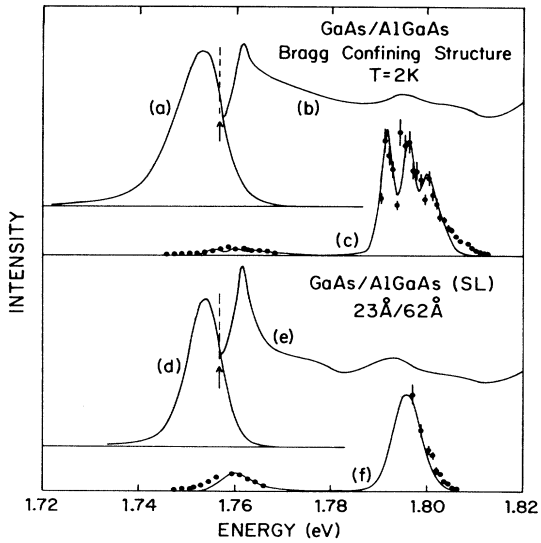

FIG. 3. A comparison between the PL spectra (curves *a* and *d*), the PLE spectra (curves *b* and *e*), and the GaAs-like LO phonon RRS profiles (curves *c* and *f*) of the finite SL sections of the BCS and the fully periodic SL. The arrows denote the monitored emission energy of the PLE spectra. The full circles are the measured integrated RRS intensities and their error bars. (In curve *f*, the low energy part of the outgoing beam resonance could not be measured because of strong overlapping luminescence.) The full lines in curves *c* and *f* are model calculations.

scattering intensity is 10^{-3} weaker than that observed for the BCS. Figure 3 shows the PL (curves *a* and *d*) and its PLE (curves *b* and *e*) spectra, in the spectral range of the $(e_1{:}hh_1)$ exciton band, for the BCS and the SL, respectively. Also shown are the GaAs-like LO phonon RRS profiles (curves *d* and *f*), measured in the same spectral range. Finally, in Fig. 4, the GaAs-like LO phonon Raman scattering spectra of the BCS are shown. Spectrum *a* is excited in the $(e_1{:}hh_1)$ exciton band, while spectrum *b* is for excitation in the $(e_B{:}hh_B)$ band. The Raman shifts of the most intense peaks (36.2 and 35.4 meV, respectively) clearly show that the phonons involved correspond to different spatial parts of the same BCS. The latter has the exact energy of the GaAs-like LO phonons in an $Al_{0.32}Ga_{0.68}As$ alloy [7].

We turn now to analyze these experimental observations. The most important result is the intense RRS which is mediated by the $(e_B{:}hh_B)$ transition (Fig. 2), and the absence of any resonant scattering in this spectral region in the case of the fully periodic SL. This serves as additional evidence for the particle Bragg confinement in the BCS barriers, and to the long dephasing time in the e_B and hh_B states. The other main result is the structure of all three RRS profiles (Fig. 2, curve *c*, and Fig. 3, curves *c* and *f*). They all consist of an intense outgoing beam resonance (OB) and a weaker incoming beam resonance (IB). The IB occurs for the exciting laser energy in the spectral range of the $1S$ exciton, at $\mathbf{K} \sim 0$ [$\mathbf{K}$ is the wave vector of the exciton center of mass (c.m.) motion], and the OB occurs when the scattered light energy is in this range. The ratio of these resonances depends on the mediating excitonic transitions: $I_{OB}/I_{IB} = 30$ for the $(e_B{:}hh_B)$ exciton band, 12 for the $(e_1{:}hh_1)$ exciton of the BCS, and 5 for this transition in the SL. As we shall presently show, these ratios depend on the $1S$ excitonic

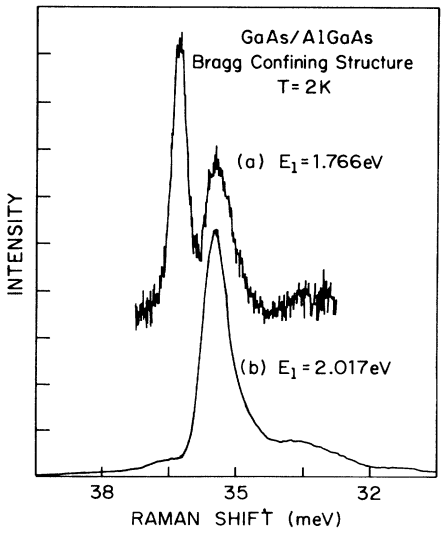

FIG. 4. A comparison between the GaAs-like LO phonon spectrum observed in two spectral regions: curve *a*, in the $(e_1{:}hh_1)$ exciton of the finite SL sections; curve *b*, in the $(e_B{:}hh_B)$ exciton.

wave function dimensionality.

In an ideal semiconductor, $I_{OB}=I_{IB}$. This is a result of the exciton **K** being a good quantum number. If interface roughness or alloy disorder is present, the exciton is scattered by the spatial potential fluctuations and $\mathbf{K}\sim 0$ states are admixed into large **K** states. Then, a double resonant enhancement occurs for the OB and $I_{OB}>I_{IB}$. Such a dependence of the I_{OB}/I_{IB} ratio on the degree of disorder was observed in bulk $Cd_xZn_{1-x}Te$ alloys [8]: For maximum disorder, namely, $x=0.5$, $I_{OB}/I_{IB}\sim 2$. Much larger I_{OB}/I_{IB} ratios have been reported for SL's and QW's [9,10], and recently this asymmetry was analyzed in terms of exciton scattering by interface roughness [11]. We shall use this approach of exciton scattering by short range potential fluctuations that can admix $1S$ states with different **K**. However, we will show that the different I_{OB}/I_{IB} ratios, observed for the three cases shown in Fig. 2, curve *c*, and Fig. 3, curves *d* and *f*, are mainly explained by variations in exciton dimensionality (since the same scattering centers are present in all cases). For the scattering potential we assume randomly distributed, uncharged point centers that represent alloy and interface fluctuations. Each center gives rise to the following perturbation Hamiltonian, operating only on the c.m. part of the exciton wave function:

$$H_s(\mathbf{R}_\parallel,Z)=V_0\delta(\mathbf{R}_\parallel-\mathbf{R}_\parallel^0)\delta(Z-Z^0)\,. \tag{1}$$

$(\mathbf{R}_\parallel^0,Z^0)$ are the position coordinates of the center and $(\mathbf{R}_\parallel,Z)$ are those of the exciton. Assuming the Born approximation, the perturbed exciton wave function which consists of a wave packet centered at $(\mathbf{K}_\parallel,K_z)$ can be formally written in terms of the unperturbed wave functions:

$$\Psi_{\mathbf{K}_\parallel,K_z}=\int_{BZ_\parallel}\frac{d^2K'_\parallel}{(2\pi)^2}\int_{BZ_z}\frac{dK'_z}{2\pi}\Psi_{\mathbf{K}'_\parallel,K'_z}[\delta(\mathbf{K}'_\parallel-\mathbf{K}_\parallel)\delta(K'_z-K_z)+g(K_\parallel,K'_\parallel,K_z,K'_z)]\,. \tag{2}$$

$g(K_\parallel,K'_\parallel,K_z,K'_z)$ is the Born propagator. Since the exciton in-plane translational mass ($M_\parallel$) is much smaller than that along the confinement direction (M_z), the propagator corresponding to H_s of Eq. (1) can be approximated by

$$g(K_\parallel,K'_\parallel)\approx\frac{2M_\parallel V_0}{\hbar^2}\frac{1}{K_\parallel^2-K_\parallel'^2}\,. \tag{3}$$

For the unperturbed $1S$ exciton envelope wave function, in all three cases described above, we use

$$\Psi^{(0)}_{\mathbf{K}_\parallel,K_z}(r_\parallel,\mathbf{R}_\parallel,z,Z)=N(\pi a_\parallel^2 a_z)^{-1/2}\exp\left\{-\left[\left(\frac{r_\parallel}{a_\parallel}\right)^2+\left(\frac{z}{a_z}\right)^2\right]^{1/2}\right\}e^{i\mathbf{K}_\parallel\cdot\mathbf{R}_\parallel}f_{K_z}(Z)\,. \tag{4}$$

N is a normalization factor. The part that depends on the relative *e*-*h* coordinates $(r_\parallel,z)$ is the commonly used [12,13] anisotropic $1S$ trial function. The ratio between the in-plane ($a_\parallel$) Bohr radius and that along the growth direction (a_z) defines the exciton dimensionality. The part that describes the exciton c.m. motion is factored into a plane wave and a wave function $f_{K_z}(Z)$ that depends on the c.m. coordinate along the confinement direction. This function is different for the three cases: For the $(e_B{:}hh_B)$ $1S$ case, $f_{K_z}(Z)$ describes an exciton that is tightly confined in the spacer layer of the BCS. For the finite SL sections of the BCS, five $f_{K_z}(Z)$ functions describe the five $(e_1(1\text{-}5){:}hh_1)$ $1S$ excitons. The splitting of these five states is resolved in the RRS profile (Fig. 3, curve *c*). For the fully periodic SL, $f_{K_z}(Z)$ has a quasicontinuous spectrum of the $(e_1{:}hh_1)$ $1S$ exciton miniband. The exact form of $f_{K_z}(Z)$ is taken as the calculated [14] electron wave function.

In a Raman scattering process, with excitation (laser) and scattered light energies and wave vectors E_l,k_l and E_s,k_s, respectively, a LO phonon is created with $\hbar\omega_{LO}(\mathbf{Q})=E_l-E_s$. The contribution of the two exciton states with energies of $E_{1S}(\mathbf{K}_\parallel=0)$ and $E_{1S}(\mathbf{K}_\parallel)=E_{1S}(\mathbf{K}_\parallel=0)+\hbar^2K_\parallel^2/2M_\parallel$ to the scattering amplitude [15] is given by

$$\begin{aligned}A(E_l,E_s,E_{1s}(0),\mathbf{Q})=A_0&\frac{1}{\pi a_\parallel^2 a_z}\frac{1}{E_lE_s}F(\mathbf{Q})\delta(E_l-E_s-\hbar\omega_{LO}(\mathbf{Q}))\\&\times\left\{\frac{\delta(\mathbf{Q}_\parallel)\delta(k_l-k_s-Q_z)}{[E_l-E_{1s}(0)+i\Gamma_{1s}(0)][E_s-E_{1s}(0)+i\Gamma_{1s}(0)]}\right.\\&+\frac{2M_\parallel V_0}{\hbar^2Q_\parallel^2}\left(\frac{1}{[E_l-E_{1s}(Q_\parallel)+i\Gamma_{1s}(Q_\parallel)][E_s-E_{1s}(0)+i\Gamma_{1s}(0)]}\right.\\&+\frac{1}{[E_l-E_{1s}(0)+i\Gamma_{1s}(0)][E_s-E_{1s}(Q_\parallel)+i\Gamma_{1s}(Q_\parallel)]}\\&\left.\left.-\frac{2}{[E_l-E_{1s}(0)+i\Gamma_{1s}(0)][E_s-E_{1s}(0)+i\Gamma_{1s}(0)]}\right)\right\}.\end{aligned} \tag{5}$$

A_0 contains all the constant factors and those that vary slowly with $K_\parallel$. $F(\mathbf{Q})$ is the Fröhlich interaction form factor, which is given by

$$F(\mathbf{Q}) = (C_F/|\mathbf{Q}|)[\alpha(\xi_e) - \alpha(\xi_{hh})] . \quad (6)$$

The function $\alpha(\xi)$ is dependent on the exciton dimensionality [12]: $\alpha(\xi) \sim (1+|\xi|^2)^{-p}$ where $p = \frac{3}{2}$ for the purely two-dimensional case, and $p=2$ in the three-dimensional case. Here $\xi_\parallel^i = m_\parallel^i a_\parallel Q_\parallel / 2M_\parallel$ and $\xi_z^i = m_z^i a_z Q_z / 2M_z$ (the index i refers to e or h). C_F is the Fröhlich interaction coupling constant. This form of $F(\mathbf{Q})$ is a slightly simplified relation based on Ref. [12].

The various exciton bands are inhomogeneously broadened: We take a Gaussian distribution $\rho(E_{1s}(0))$ (with a width $2\sqrt{\ln 2}\Delta$) for the spectral distribution of E_{1s}. The damping factors, Γ_{1s}, have a spectral distribution over the exciton band. However, the calculated RRS profiles can be well fitted to the experimental ones assuming a single Γ for each of the excitonic bands shown in Figs. 2 and 3. It is seen that a double resonance is obtained when $E_l - E_{1S}(\mathbf{Q}_\parallel) = \hbar\omega_{\mathrm{LO}}(\mathbf{Q})$ [the second term in Eq. (5)]. The RRS profile is then given by

$$\sigma(E_l) = \sigma_0 \int_{BZ_\parallel} \frac{d^2Q_\parallel}{(2\pi)^2} \int_{BZ_z} \frac{dQ_z}{(2\pi)} \int dE_{1s}(0)\rho(E_{1s}(0)) |A(E_l, E_l - \hbar\omega_{\mathrm{LO}}(\mathbf{Q}), E_{1s}(0), \mathbf{Q})|^2 . \quad (7)$$

TABLE I. The parameters used in fitting the RRS profiles.

Structure	Exciton type	Γ_{1s} (meV)	$\sqrt{\ln 2}\Delta$ (meV)	$a_\parallel$ (Å)	a_z (Å)
BCS	$(e_B{:}hh_B)$	0.20	4.5	50	6
BCS	$(e_1(1){:}hh_1)$	0.20	2.0	60	10
BCS	$(e_1(2){:}hh_1)$	0.20	2.0	60	10
BCS	$(e_1(3){:}hh_1)$	0.21	2.0	60	10
BCS	$(e_1(4){:}hh_1)$	0.25	2.0	60	10
BCS	$(e_1(5){:}hh_1)$	0.40	2.0	60	10
SL	$(e_1{:}hh_1)$	0.20	3.5	60	20

The calculated $\sigma(E_l)$ are shown by the solid lines in Fig. 2 and Fig. 3, curves c and f. The in-plane e and h masses used in the calculation of all three RRS profiles are [16,17] $m_{e\parallel} = 0.07m_0$ and $m_{hh\parallel} = 0.15m_0$. The value of V_0 [in Eq. (1)] is taken as 0.1 eV. All the other parameters obtained by fitting the model to the observed profiles are listed in Table I. (The sensitivity of the parameters to the best fit is $\pm 15\%$.)

The main conclusion to be drawn from the good fit to the experimental RRS profiles concerns the exciton dimensionality. The large anisotropy in the $(e_B{:}hh_B)$ $1S$ exciton ($a_\parallel/a_z \sim 8$) indicates that this exciton is virtually two dimensional. The calculated [1] confinement factor of both e_B and hh_B is 0.97 and 0.91, respectively. These are similar to the confinement factor calculated [13] for $(e_1{:}hh_1)$ $1S$ excitons in conventional GaAs/AlGaAs QW's. In that case, the calculated $a_\parallel/a_z$ is ~ 4.5, for a well width similar to the Bragg confining spacer layers studied here. From this we conclude that the exciton dimensionality is largely determined by the degree of confinement. As the degree of confinement decreases, and the exciton wave function spreads over larger distances, its dimensionality approaches 3: In the finite SL sections $a_\parallel/a_z = 6$ and in the fully periodic SL $a_\parallel/a_z = 3$. We also found that the LO phonon spectra, observed by the RRS in the two exciton bands of the BCS, are different. The phonon energies are those of the AlGaAs alloy for the Bragg confined excitons and of GaAs for the SL sections. This serves as a clear indication of the distinct spatial confinement regions of the excitons involved in the RRS.

The research at Technion was supported by the U.S.-Israel Binational Science Foundation (BSF), Jerusalem, Israel, and was done in the Center for Advanced Opto-Electronics. E. Linder acknowledges the support of the Center for Absorption in Science, Ministry of Immigrant Absorption, State of Israel.

[1] M. Zahler, I. Brener, G. Lenz, J. Salzman, and E. Cohen, Appl. Phys. Lett. **61**, 949 (1992).
[2] F. C. Zhang, N. Dai, H. Luo, N. Samarth, M. Dobrowolska, J. K. Furdyna, and L. R. Ram-Mohan, Phys. Rev. Lett. **68**, 3220 (1992).
[3] C. Sirtori, F. Cappaso, J. Faist, D. L. Sivco, S-n. G. Chu, and A. Y. Cho, Appl. Phys. Lett. **61**, 898 (1992).
[4] F. Capasso, C. Sirtori, J. Faist, D. L. Sivico, S. Nee, G. Chu, and A. Y. Cho, Nature (London) **358**, 565 (1992).
[5] F. H. Stillinger, Physica (Amsterdam) **85B**, 270–276 (1977).
[6] G. Lenz and J. Salzman, Appl. Phys. Lett. **56**, 871 (1990).
[7] S. Adachi, J. Appl. Phys. **58**, R1 (1985).
[8] I. Brener, E. Cohen, A. Muranevich, and R. Triboulet, Phys. Rev. B **40**, 8313 (1989).
[9] I. Brener, E. Cohen, A. Ron, and L. N. Pfeiffer, Superlattices Microstruct. **5**, 223 (1989).
[10] A. J. Shields, M. Cardona, R. Nötzel, and K. Ploog, Phys. Rev. B **46**, 10490 (1992).
[11] A. J. Shields, C. Trallero-Giner, M. Cardona, H. T. Grahn, K. Ploog, V. A. Haisler, D. A. Tenne, N. T. Moshegov, and A. I. Tropov, Phys. Rev. B **46**, 6990 (1992).
[12] T. Takagahara, Phys. Rev. B **31**, 6552 (1985).
[13] M. Grundmann and D. Bimberg, Phys. Rev. B **38**, 13486 (1988).
[14] Full details on the calculations of the Bragg confined e and h wave functions and of the RRS profiles will be published elsewhere.
[15] R. M. Martin, Phys. Rev. B **4**, 3676 (1971).
[16] S. Datta, in *Modular Series on Solid State Devices,* edited by R. F. Pierret and G. W. Neudeck, Quantum Phenomena Vol. VIII (Addison-Wesley, Reading, MA, 1989), p. 200.
[17] L. C. Andreani and A. Pasquarello, Phys. Rev. B **42**, 8928 (1991); L. C. Andreani, Ph.D. thesis, Scuola Normale Superiore, Pisa, 1989.